Ionomeric Blends of Poly(ethyl acrylate-*co*-4-vinylpyridine) with Metal-Neutralized Sulfonated Poly(ethylene terephthalate). 4. Effects of Counterions

C.-W. Alice Ng and William J. MacKnight*

Department of Polymer Science and Engineering, University of Massachusetts, Amherst, Massachusetts 01003

Received July 10, 1995; Revised Manuscript Received November 20, 1995[⊗]

ABSTRACT: This is the fourth part in a series of studies on the ionomer blend system of poly(ethyl acrylate-*co*-4-vinylpyridine) with metal-neutralized sulfonated poly(ethylene terephthalate). The focus of this work was to investigate the influence of counterions of the ionomers on the phase behavior and the ultimate mechanical properties of the blend system. The counterions examined included the group I and II metals Li^+, Na^+, and Ca^{2+} and the transition metals Co^{2+}, Ni^{2+}, Cu^{2+}, and Zn^{2+}. Specific interactions between the different metal-neutralized sulfonate groups and the vinylpyridine groups were proven by FTIR spectroscopy to exist for the transition metal counterions. As a result of these specific intermolecular interactions, compatible blends were achieved with the transition metal counterions whereas the group I and II counterions showed total immiscibility as evidenced by the glass transition behavior probed by differential scanning calorimetry (DSC) and dynamic mechanical thermal analysis (DMTA). In addition, the mechanical properties of the compatible blends were significantly better than those of the immiscible blends, probably due to the lack of interfacial adhesion in the latter. The modulus and tensile strength of the Ca^{2+}-containing blend showed some enhancement compared to the group I metal-containing blends, and this could arise from the presence of some interfacial interactions in it. The degree of property enhancement was found to be a complex function of the nature, strength, and extent of the transition metal complexation between the polymeric components. The crystalline phase in terms of the crystallization kinetics and crystalline morphology of the PET ionomers was strongly influenced by the presence of different counterions and their interactions with the vinylpyridine-containing polymer. The observed modifications provide indirect evidence for the compatibility of the blend system.

Introduction

This report is a continuation of the study on the ionomer blend system of poly(ethyl acrylate-*co*-4-vinylpyridine) (EAVP) with sulfonated poly(ethylene terephthalate) (PET-SO_3M).[1−3] The motivation is to use specific interactions between the polymer pair to form miscible or compatible blends. Miscibility in this context refers to a one-phase blend in the thermodynamic sense, while compatibility refers to a two-phase blend in which interactions between the phases (perhaps interfacial adhesion) lead to an enhancement of properties. The strategy used is to incorporate a small amount of ionic or polar moieties into both polymer chains so that they are capable of specifically interacting with each other to enhance mixing. Hence we examine the influence of counterions on the behavior of the PET-SO_3M and its compatibility with EAVP. The selection of counterions, Li^+, Na^+, and Ca^{2+} from groups I and II and Co,$^{2+}$ Ni^{2+}, Cu^{2+}, and Zn^{2+} from the transition metal series, allows a systematic comparison of the types of interactions occurring between the incorporated functional groups.

Numerous studies have focused on blends of pyridine-containing polymers with ionomers where the pyridine nitrogen provides a basic site for acid/base interactions and a basic ligand for transition metal coordination with ion-containing polymers. Agarwal et al. described the rheological and mechanical properties of blends of styrene−vinylpyridine copolymer (SVP) with sulfonated ethylene−propylene−diene elastomer (S-EPDM).[4,5] It was found that these properties were influenced strongly by the coordination between the transition metal counterions of the S-EPDM and the pyridine nitrogen while almost no effects were observed with counterions such as Na and Mg. On the other hand, Lu and Weiss examined the solution behavior of SVP with sulfonated polystyrene.[6] They found that in addition to the strong coordination observed with transition metal cations, both alkaline and alkaline earth metal cations also exhibit some interactions in the solution state. Belfiore et al. studied blends of poly(vinylpyridine) (PVP) with several transition metal acetates.[7−9] They observed enhancement in the glass transition temperature (T_g) for blends with cobalt, nickel, and zinc acetates. The greatest enhancement was found with the nickel acetate blend, with an increase of 100 °C from the T_g of the PVP, and they attributed this result to the energetic stabilization due to the ligand field.[8] This body of work has demonstrated successfully the various interactions existing between the pyridine and different metal-neutralized sulfonate and acetate functional groups and their influence on the resulting properties of different polymer blend systems.

In this work, the counterion effects on the compatibility behavior of the EAVP/PET-SO_3M blends and their ultimate mechanical properties are investigated. The specific intermolecular interactions between the blend components is examined by FTIR spectroscopy. Thermal analysis by DSC and DMTA is employed to measure the glass transition behavior of the blends and hence their compatibility. The influence of blend mixing on the crystallization behavior of the semicrystalline ionomer component is investigated by examining the crystallization kinetics and its resulting melting behavior before and after blending. Finally, the ultimate tensile properties of the blends and their fracture morphologies are examined.

[⊗] Abstract published in *Advance ACS Abstracts,* February 1, 1996.

0024-9297/96/2229-2421$12.00/0

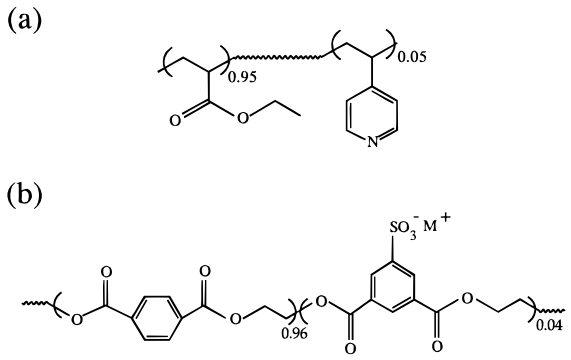

Figure 1. Chemical structures of (a) 5EAVP and (b) 4PET-SO_3M.

Table 1. Nomenclature and Compositions of Polymer Blends

polymer	designation	wt % 5EAVP	wt % 4PET-SO_3M
5EAVP/4PET-SO_3Li-45/55	5B-Li	45	55
5EAVP/4PET-SO_3Na-45/55	5B-Na	45	55
5EAVP/4PET-SO_3Ca-45/55	5B-Ca	45	55
5EAVP/4PET-SO_3Co-45/55	5B-Co	45	55
5EAVP/4PET-SO_3Ni-45/55	5B-Ni	45	55
5EAVP/4PET-SO_3Cu-45/55	5B-Cu	45	55
5EAVP/4PET-SO_3Zn-45/55	5B-Zn	45	55

Experimental Section

Materials Used. Poly(ethyl acrylate-*co*-4-vinylpyridine) with 5 mol % of vinylpyridine content, denoted as 5EAVP, was prepared by free-radical polymerization as reported.[10] The number-average molecular weight was found to be 201 000 with a polydispersity of 2.02. Sodium-neutralized sulfonated poly(ethylene terephthalate) with 4 mol % sulfonation level, denoted as 4PET-SO_3Na, was kindly supplied by AKZO Corporate Research, Arnhem, Holland. The sulfonation level was further confirmed by elemental analysis.[11] The inherent viscosity of the 4PET-SO_3Na was found to be 0.45 dL/g measured in trifluoroacetic acid at 30 °C as previously reported.[3] The chemical structures of both polymers are schematically shown in Figure 1. All other chemicals were purchased from Aldrich Chemical Co., and they were used without further purification.

Ion Exchange Procedure. An ion exchange procedure was developed to exchange the initial sodium ions of the sulfonated PET for hydrogen ions and subsequently for zinc ions.[1] Due to the unique heterogeneous nature of the process, it can be applied to neutralize sulfonated PET with a wide range of metal ions without concern about the solubility problems usually associated with the homogeneous neutralization process. In this study, aside from using the zinc acetate solution (1.4 M) as a source of metal ion, lithium acetate (1.47 M), calcium acetate (1.5 M), cobalt acetate (1 M), nickel acetate (0.8 M), and copper acetate (0.4 M) solutions were employed as the neutralizing agents with concentrations ranging from 0.4 to 1.5 M as indicated depending upon the solubility of the metal salt. The metal-neutralized polymers, 4PET-SO_3M, were then subjected to elemental analysis[11] to confirm complete conversion of the 4PET-SO_3Na to the desired metal salt form.

Blend Preparation. The 5EAVP and 4PET-SO_3M were solution blended in 1,1,1,3,3,3-hexafluoro-2-propanol (HFIP). The functionalization levels of both polymers were kept constant. Also, the stoichiometry between the vinylpyridine and the sulfonate interacting groups was maintained in all the blends. (In this regard, no distinction was drawn between monovalent and divalent cations. Stoichiometry here means a 1:1 ratio of sulfonate group to vinylpyridine.) The nomenclature and compositions of the blends prepared are listed in Table 1.

Individual homopolymers were predried at 60 °C for 1 day under vacuum prior to use. The constituent polymers were dissolved separately in HFIP to yield a 5% (w/v) polymer solution. The 5EAVP solution was then added to the 4PET-SO_3M solution under vigorous stirring. Due to gelation occurring in some of the blends, all blend solutions were further heated at 70 °C for 5 h in a nitrogen atmosphere to ensure thorough mixing. The blend solution was then cast onto a Teflon dish under a slow stream of nitrogen. After most of the solvent was removed at ambient conditions, the polymer film was allowed to dry at 60 °C for 3 days under vacuum.

FTIR Study. Infrared spectra were obtained on an IBM IR44 FTIR spectrometer. A total of 128 scans at a resolution of 1 cm^{-1} were signal averaged. Thin films were prepared by dissolving the sample in HFIP at a concentration of 4% (w/v) and casting onto a flat Teflon sheet under a slow stream of nitrogen. The films were further dried at 60 °C for 3 days under vacuum.

DSC Measurements. A Perkin-Elmer DSC-7 was used to obtain DSC thermograms and was calibrated with indium and water. Experiments were run with samples ranging from 5 to 10 mg under a dry nitrogen purge to prevent moisture and oxidative degradation. To obtain the thermal behavior of the as-cast films, the samples were equilibrated at −50 °C and heated to 250 °C at 10 °C/min. Quenched samples of both the blends and the constituent polymers were obtained by heating at 250 °C for 5 min and quenching at a nominal rate of 500 °C/min to −50 °C. The thermal behavior of the quenched samples was probed by heating and cooling between −50 and 250 °C at a rate of 10 °C/min. The glass transition temperatures (T_g) were taken as the midpoints of the change in heat capacity. The melting temperatures (T_m) and the crystallization temperatures (T_c) were taken as the peaks of the transitions. The heat of fusion (ΔH_m) and heat of crystallization (ΔH_c) were measured by calculating the area under the appropriate endothermic or exothermic peaks and were normalized per gram of the semicrystalline component in the blends. The percent crystallinity of the crystallized samples was estimated by assuming an enthalpy of melting of 113 J/g for 100% crystalline PET.[12]

The crystallization rates of both the blends and the 4PET-SO_3M homopolymers were measured at T_c = 150 °C. The samples were treated at 250 °C for 5 min and were quenched to T_c at a nominal rate of 500 °C/min in the DSC. The crystallization was allowed to proceed for an hour. The crystallization isotherm was recorded and the crystallization half-time ($t_{1/2}$) was determined as described in a previous publication.[2] The melting behavior of the isothermally crystallized samples was obtained by heating directly from T_c to 250 °C at a rate of 10 °C/min.

DMTA Measurements. Dynamic mechanical properties were measured using a Polymer Laboratories PL-DMTA instrument at a frequency of 1 Hz. Quenched blends were prepared by compression molding under low pressure and a nitrogen atmosphere at 250 °C for 1 min and cooling quickly between two cold metal plates. The 5EAVP polymer was compression-molded under similar conditions between sheets of aluminum foil at 50 °C. The solution-cast blend samples were cut into appropriate sizes and examined as-cast. Due to the brittleness of the 4PET-SO_3M polymers, films could not be prepared. All specimen sizes were approximately 25 mm × 13 mm × 0.5 mm. Experiments were performed in a single-cantilever mode using a 5.2-mm free length and were scanned from −100 to +200 °C at a rate of 3 °C/min. The T_g's were taken as the peaks in the tan δ plots. The modulus data were treated with the PL-DMTA end correction software to correct for sample clamping efficiency.

Tensile Measurements. Uniaxial stress−strain data were obtained with an Instron Model 4202 Testing Instrument equipped with a Series IX automatic materials testing system for automatic data acquisition. Solution cast samples were used and cut into thin strips of approximately 6 mm × 0.5 mm × 80 mm. Experiments were run with an initial gauge length of 40 mm at a constant crosshead speed of 4 mm/min at room temperature. Three to five samples were examined for each material and the results averaged.

SEM Measurements. A JEOL JSM-35CF scanning electron microscope operating at 20 kV was used to examine

Table 2. Experimental Observations during Blending Mixing

metal	metal salt	metal-neutralized sulfonated PET	5B-M blends	solution viscosity in HFIP
Li	CH_3COOLi (white)	white	white	+
Na		white	white	+
Ca	$(CH_3COO)_2Ca$ (white)	white	white	+
Co	$(CH_3COO)_2Co$ (pink)	light pink	blue	++
Ni	$(CH_3COO)_2Ni$ (green)	greenish gray	pale green	+++
Cu	$(CH_3COO)_2Cu$ (deep blue)	light green	blue	++++
Zn	$(CH_3COO)_2Zn$ (white)	white	white	+++

fracture surfaces. Solution cast samples were freeze fractured at liquid nitrogen temperature. The sample surfaces were coated with a thin layer of gold for examination under the microscope.

Results and Discussions

Choice of Counterions. Specific intermolecular interactions are known to play an important role in controlling the phase behavior of ionomeric blend systems. The extent, the nature, and the strength of the interactions are among the variables critical in determining the mixing behavior of polymeric components containing ionic and/or polar species. There are two types of specific interactions that are of interest in the 5EAVP/4PET-SO_3M blend system: (a) the ion-pair or multiplet interactions[13] within the PET ionomer and (b) the interactions between the metal-neutralized sulfonate groups in the PET chains and the vinylpyridine groups in the poly(ethyl acrylate) chains. The relative extent of interactions (a) and (b) is controlled in part by the type of counterions used in the ionomer, and this will ultimately determine the amount of mixing between the two polymers. Hence, in this study, a variety of counterions are selected to examine their influence on the nature and strength of interactions occurring among the blend components. Special attention is focused on the transition metals because of their strong coordination affinities for vinylpyridine.

Table 2 summarizes the changes in color and the qualitative differences in viscosity during the blending of the various PET-SO_3M's with EAVP. It is found that at equal concentrations of the blend solutions, different levels of gelation are observed depending upon the counterions used. The solution viscosity is generally much higher among the mixtures containing transition metal ions as the counterions compared to those containing group I and II metal ions. Such differences in the solution viscosity provide evidence that the effective molecular weight of the system has changed as a result of the different level of interactions. On the other hand, the change in color between the transition metal-neutralized ionomers and the blends suggests that there is an exchange of ligands that are coordinated to the transition metal. Depending upon the coordination capacity of the transition metal, a different level of gelation is observed. It is of importance that the above observations provide macroscopic although qualitative evidence about the influence of counterions upon the structure and properties of an ionomeric blend system.

Specific Intermolecular Interactions. Figure 2 shows the IR spectra for 5EAVP, PET, and the 5B-M blends. Previous findings[1] indicate that the peak at 1600 cm^{-1} corresponds to the free pyridine ring stretching whereas the peak at 1620 cm^{-1} is attributed to the pyridine ring stretching coordinated with zinc ions. The relative peak intensity at 1600 cm^{-1} exhibited by the blends reveals higher levels of interactions at the pyridine ring among the transition metal containing

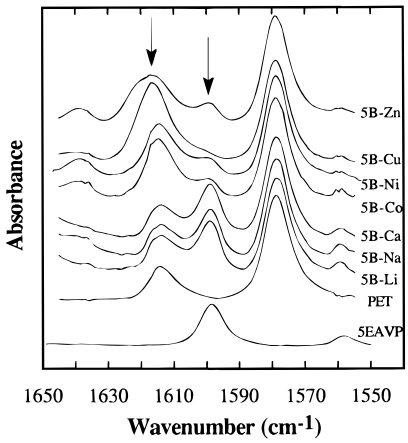

Figure 2. FTIR spectra for 5EAVP, PET, and 5B-M blends.

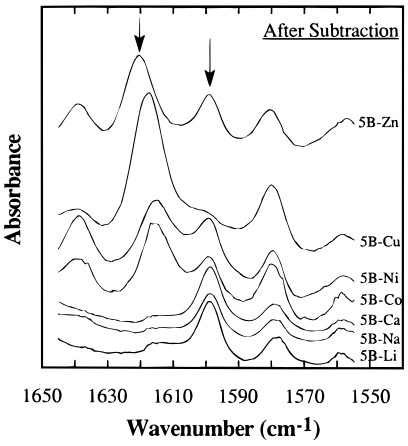

Figure 3. FTIR spectra for 5B-M blends after subtraction; the subtraction was performed based on the peak at 1580 cm^{-1}.

blends as compared to those of the non-transition metal containing blends. In particular, the 5B-Cu blend shows almost complete interactions at the pyridine functional groups. In the case of the reacted pyridine ring, its peak is likely overlapped with a small peak at 1615 cm^{-1} which is contributed by the PET component.[3] Therefore, a subtraction procedure is carried out on the spectra of the blends to remove the noninteracting component from the complexed pyridine ring peak at 1620 cm^{-1} as shown in Figure 3. The subtracted spectra of the 5B-Li, 5B-Na, and 5B-Ca blends clearly reveal that there is no interaction between the pyridine ring and these cations. This is expected because these group I and II cations are oxophilic in nature and have no tendency to interact with pyridine nitrogen. However, in the case of the 5B-Co, 5B-Ni, 5B-Cu, and 5B-Zn blends, a new absorption peak is observed at a higher frequency relative to that of the free pyridine ring stretching. Based on the previous findings, this new peak is ascribed to the coordination of the pyridine ligand (py) to the transition metal ion. It is known that the lone pair of electrons on nitrogen represents a strong

Table 3. FTIR Results: Peak Assignments for Pyridine Ring Stretching in the 1650−1550 cm^{-1} Region

polymer	peak$_{complex}$ (cm^{-1})	peak$_{free}$ (cm^{-1})
5B-Li		1600
5B-Na		1600
5B-Ca		1600
5B-Co	1615	1600
5B-Ni	1615	1600
5B-Cu	1618	1600
5B-Zn	1620	1600

Table 4. DSC Results: T_g's of the 5EAVP/4PET-SO$_3$M-45/55 and Their Constituent Polymers in the Quenched State

polymer	T_{g1} (°C)	ΔT_{g1} (°C)	T_{g2} (°C)	ΔT_{g2} (°C)
5B-Li	−10	8	65	7
5B-Na	−11	8	62	8
5B-Ca	−11	8	61	10
5B-Co	−10	12	57	11
5B-Ni	-10	14	57	11
5B-Cu	−7	18	57	11
5B-Zn	−10	13	57	14
5EAVP	−12	5		
4PET-SO$_3$Li			63	11
4PET-SO$_3$Na			62	9
4PET-SO$_3$Ca			64	6
4PET-SO$_3$Co			65	7
4PET-SO$_3$Ni			66	7
4PET-SO$_3$Cu			67	6
4PET-SO$_3$Zn			64	8

basic ligand for coordination to transition metals. A close examination of the spectra reveals that the vibrational frequency ν of the coordinated ligand exhibits a slight dependence on the transition metals: $\nu_{(Zn\text{-}py)}$, $\nu_{(Cu\text{-}py)} > \nu_{(Ni\text{-}py)}$, $\nu_{(Co\text{-}py)} > \nu_{(py)}$, as illustrated in Table 3. Such frequency dependence could be explained based on the fact that the larger the frequency shift from that of the free ligand, the stronger is the coordination of the ligand (or specifically the lone pair of electrons on the nitrogen atom) to the transition metal, if the reduced mass of the vibration remains the same, which is true in this case as the masses of the transition metals are very similar. Therefore, the strength of the interaction between the ligand and the transition metal ion is expected to correlate with the complexed pyridine ring stretching vibration frequency. On the other hand, the coexistence of the free pyridine ring stretching peak with that of the complexed ring clearly indicates that the reaction between pyridine and the transition metal remains incomplete, despite the 1:1 stoichiometry of both functional groups.

Compatibility Behavior. Table 4 summarizes the T_g measurements of the quenched 5B-M blends and their corresponding homopolymers as probed by DSC. It is shown clearly that all the blends are immiscible with two phases displaying two T_g's. In case of the EAVP phase of the blends, both the T_{g1} and ΔT_{g1} of the 5B-Li, 5B-Na and 5B-Ca blends show no significant changes as compared to the 5EAVP homopolymer. Similar behavior is observed for the sulfonated PET phase of these blends. This suggests that the degree of phase mixing is very low, if not totally nonexistent. The poor mixing behavior is in accord with the FTIR studies, which indicate that no specific interactions occur between the two polymeric components. On the other hand, all the transition metal containing blends show that the T_g's of the EAVP phase do not show significant changes as compared to the 5EAVP homopolymer except that of the 5B-Cu blend. However, they all exhibit a substantial broadening. The T_g's of the sulfonated PET phase show a decrease of about 10 °C with moderate broadening. These results suggest considerable interfacial mixing in these blends and also the presence of a nearly pure EAVP phase (except for 5B-Cu, which shows a mixed EAVP phase) and a mixed PET-SO$_3$M phase. In other words, the specific interactions present in the blends with transition metal cations lead to favorable phase mixing, the extent of which is determined by the particular cation present.

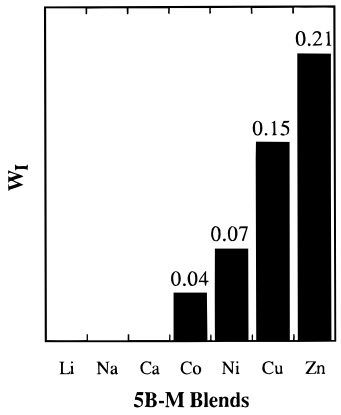

Figure 4. Extent of interfacial mixing W_I of the 5B-M blends based on phase composition calculation.

The degree of interfacial mixing in the compatible blends can be estimated according to the equation proposed by MacKnight et al[14]:

$$W_I = 1 - \frac{\Delta C_{p2}[\Delta C_{p2}^{\circ} \ln(T_{g2}^{\circ}/T_{g2}) - \Delta C_{p1}^{\circ} \ln(T_{g1}^{\circ}/T_{g2})]}{\Delta C_{p1}^{\circ}\Delta C_{p2}^{\circ} \ln(T_{g2}^{\circ}/T_{g1}^{\circ})} - \frac{\Delta C_{p1}[\Delta C_{p2}^{\circ} \ln(T_{g2}^{\circ}/T_{g1}) - \Delta C_{p1}^{\circ} \ln(T_{g1}^{\circ}/T_{g1})]}{\Delta C_{p1}^{\circ}\Delta C_{p2}^{\circ} \ln(T_{g2}^{\circ}/T_{g1}^{\circ})} \quad (1)$$

where W_I is the weight fraction of the blend constituents comprising the interphase of a microphase-separated amorphous polymer blend; T_{g1}^{o} and T_{g2}^{o} are the T_g's of the constituents before mixing; T_{g1} and T_{g2} are the T_g's of the constituents after mixing; ΔC_{p1}^{o} and ΔC_{p2}^{o} are the step increases in heat capacity at the T_g's of the constituents before mixing; and ΔC_{p1} and ΔC_{p2} are the corresponding step increases in heat capacity in the blend.

The results of the extent of interfacial mixing are illustrated in Figure 4. It should be noted that the calculation is based on a number of simplifying assumptions, including the representation of a compatibilized blend as a three-phase material (two bulk phases and an interphase), and that the compositional gradient across the interphase is linear. The values shown in Figure 4 are therefore valid for comparison purposes only. Thus, according to the calculation, the 5B-Li, 5B-Na, and 5B-Ca blends exhibit essentially no interfacial mixing whereas the transition metal containing blends show an increase in the quantity of interfacial material in the order 5B-Co < 5B-Ni < 5B-Cu < 5B-Zn. It is interesting to note that this trend correlates with the strengths of the interactions between the pyridine and the transition metal cation as shown in the FTIR studies.

The compatibility behavior of the 5B-M blends is further examined by DMTA. Figure 5 shows the temperature dependence of tan δ of the blends in both the

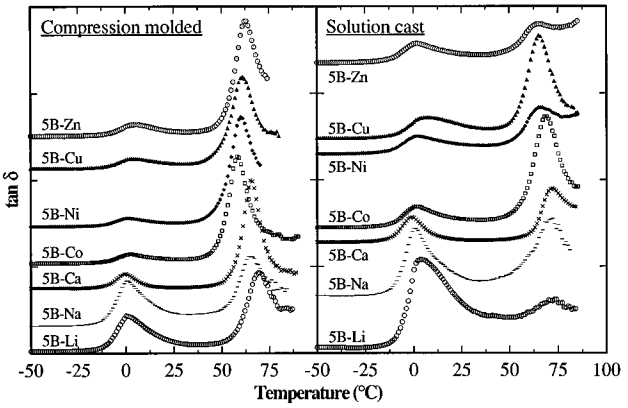

Figure 5. Temperature dependence of tan δ for the compression-molded and solution-cast blends of 5B-M recorded at 1 Hz at a scan rate of 3 °C/min.

amorphous/amorphous (compression-molded) and the semicrystalline/amorphous (solution-cast) states. The tan δ curves are typical of two-phase systems showing both the rubbery phase (5EAVP) and the glassy phase (PET-SO_3M) transitions. It is observed that the rubber damping amplitude varies among the blends despite the fact that all blends contain the same amount of rubber content. As shown from the tan δ plots, the rubber damping amplitude is low among the transition metal containing blends compared to the 5B-Li and 5B-Na blends, while the 5B-Ca blend lies in between the two groups. As suggested by McCrum,[15−17] the amplitude of the rubber damping peak is influenced by the quantity of rubber active in the transition. In other words, the change in the damping amplitude can be attributed to the different level of mechanical coupling between the rubber and the glassy phases. For instance, a blend system with poor interfacial adhesion would result in the mechanical isolation of the rubbery phase from the high modulus glassy matrix and thus give rise to a strong damping effect as much of the rubber component becomes active in the relaxation as in the case of the 5B-Li and 5B-Na blends. A pronounced increase in the damping amplitude of the rubbery phase is further observed for the 5B-Li and 5B-Na blends when the glassy phase is crystallized. This is probably due to a further mechanical isolation of the rubbery phase in the blend matrix as a result of the crystallization. However, the presence of specific intermolecular interactions leading to a substantial mixed interphase as shown in the transition metal containing blends leads to a strong coupling between the rubbery phase and the glassy matrix, which results in a reduction in the damping amplitude. It is further noted that this coupling is not affected by the crystallization of the glassy phase as shown in the solution-cast samples. In the case of the 5B-Ca blend, despite the absence of specific interactions as observed by FTIR studies and the poor phase mixing as shown by DSC studies, the lower rubber damping amplitude as compared to the 5B-Li and 5B-Na blends might suggest a certain degree of interfacial adhesion occurring in the blend matrix. The probable reason for this is that there might be a certain amount of ion−dipole interactions present at the interface as a result of the high charge density of Ca^{2+}.

Table 5 summarizes the tan δ data for the 5EAVP homopolymer and the blends. The T_g of the rubbery phase of the quenched blends, T_{g1}, shows a slight increase in the transition metal containing blends as compared to the 5EAVP homopolymer while no change is observed with the non-transition metal containing blends. These results correlate well with the trends observed by DSC. Upon crystallization of the glassy phase, the rubbery phase responds differently among the blends in that some show an increase in T_g while others exhibit a decrease as compared to their quenched counterparts. The reason for such changes is not well understood. However, it appears that the change in T_g of the rubbery phase is not as important as the change in the damping amplitude in characterizing the phase interaction between the rubbery and the glassy phases in particular for compatibilized blend systems. In addition, the substantial broadening of the glass transition of the rubbery phase relative to the 5EAVP homopolymer indicates the presence of interfacial mixing in all the blends. However, the DMTA results provide no conclusive evidence on the relative degree of mixing at the interface as effected by the different counterions. In the case of the glassy phase of the blends, the T_g shifts to higher temperatures in the solution-cast samples as compared to their compression-molded counterparts. This has been shown to be related to the stiffening effect imposed on the amorphous glassy phase by its neighboring crystallized component as typically observed for crystallized PET.[2] The extent of the shift in T_g is dependent upon the amount of crystallinity developed during the solution-casting process which is in turn related to the type of counterions present in the matrix as will be discussed later. Furthermore, a corresponding decrease in the damping amplitude of the glassy phase is observed as a result of the depletion of the amorphous components participating in the glassy phase transition.

Mechanical Properties. Figure 6 shows the storage modulus (E′) of both the compression-molded and solution-cast blends as a function of temperature. In the temperature region between the rubbery and glassy phase transitions (10−30 °C), the moduli of the 5B-Li

Table 5. DMTA Results: tan δ for 5EAVP Homopolymer and the 5B-M Blends in the Quenched and Solution-Cast States

	quenched				solution-cast				
	tan δ_{peak} (°C)		peak width at half-height (°C)		tan δ_{peak} (°C)		peak width at half-height (°C)		%
polymer	T_{g1}	T_{g2}	ΔT_{g1}	ΔT_{g2}	T_{g1}	T_{g2}	ΔT_{g1}	ΔT_{g2}	crystallinity[a]
5B-Li	0	70	21	20	4	73	29	45	22
5B-Na	0	65	19	21	0.5	72	17	22	21
5B-Ca	0	65	12	11	−1	72	13	20	24
5B-Co	3	58	24	14	1	69	24	17	27
5B-Ni	1	60	23	17	2	66	30	34	27
5B-Cu	4	61	27	15	7	65	36	16	24
5B-Zn	5	63	23	15	2	65	26	37	27
5EAVP	1		10						

[a] % crystallinity obtained from DSC studies.

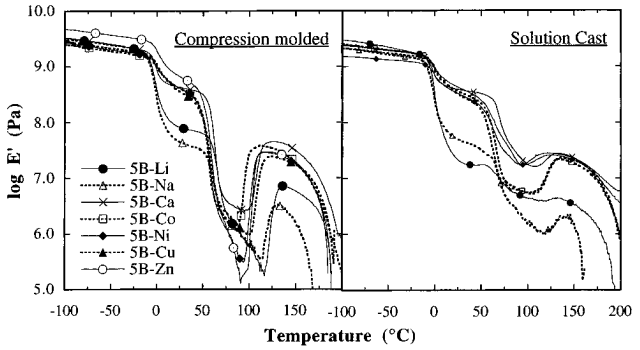

Figure 6. Temperature dependence of storage modulus (log E') for the compression-molded and solution-cast blends of 5B-M recorded at 1 Hz at a scan rate of 3 °C/min.

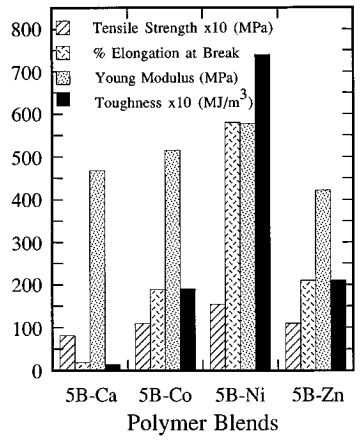

Figure 7. Comparison of the tensile properties of solution-cast blends of 5B-Ca, 5B-Co, 5B-Ni, and 5B-Zn.

and 5B-Na blends are an order of magnitude lower than the group of blends containing the divalent counterions. The large difference between the two groups can be explained by the presence of interfacial adhesion, which allows reinforcement of the glassy matrix by the rubbery component. Besides, the result might also imply a significant change in the blend morphologies as a result of the specific interactions in which the 5B-Li and 5B-Na blends show a dispersion of the glassy phase in the rubbery phase while other blends exhibit a nearly cocontinuous phase. Further evidence could be found in the fracture surface morphologies discussed in a later section. In the plateau region ranging from 110 to 200 °C, a similar difference in modulus is observed, which is again attributed to a stronger physical cross-link network sustained by favorable interfacial adhesion. On the other hand, the comparison between the compression-molded and solution-cast samples reveals little difference in the temperature dependence of E', except for an extended plateau region exhibited by the solution-cast blends. This may be ascribed to the emergence of an interconnecting crystalline domain among the amorphous components in the solution crystallized case.

Figure 7 summarizes the tensile properties of selected blends. The 5B-Li and 5B-Na blends were not examined due to their poor specimen qualities (such as uneven film thickness and poor mechanical integrity). The 5B-Cu blend shows promising tensile properties; however, good tensile specimens could not be obtained due to its unusually viscous solution mixture, which made it impossible to avoid air bubbles during film formation. Both the Young's modulus and the tensile strength show little variation among the blends examined. Similar behavior has been observed with the room temperature storage modulus which involves small strain measurements. However, the large deformation behavior (the toughness and the percent elongation at break) show dramatic variations among the blends. The 5B-Ni blend sustains the largest elongation up to 600% and has the highest toughness value. The inferior performance of the 5B-Ca blend is predictable because of the lack of strong specific intermolecular interactions and poor phase mixing. However, it may seem contradictory that its modulus and tensile strength are as high as those of the transition metal containing blends. This might be attributed to the presence of a certain amount of ion−dipole interactions at the interface as a result of the high charge density of Ca^{2+} as previously proposed. However, the short-range ion−dipole interactions are not strong enough to sustain large deformations of the matrix and thus lead to early brittle failure in the tensile measurements. On the other hand, the dramatic increases in the elongation at break and toughness in the transition metal containing blends as compared to their non-transition metal counterparts appears to be a manifestation of the strength of the interfacial adhesion as a result of the formation of coordination complexes in the former. The almost threefold increase in the elongation at break of the 5B-Ni blend is quite unexpected on this basis, however. The strength of the interactions in the 5B-Ni blend as assessed by the frequency of the complexed pyridine IR stretching vibration is comparable to that of Co and less than that of Zn (Table 3). Further, the degree of interfacial mixing as judged from the fraction of material present at the interface is much less for Ni than Zn (Figure 4). At this stage, the origin of such synergistic property enhancement exhibited by the 5B-Ni blend is not well understood. However, based on the evidence obtained, it is speculated that an optimum combination of the amount of interfacial adhesion, the extent and strength of the specific interactions, might be partially responsible for the exceptional tensile performance of the 5B-Ni blend. More importantly, such findings have led to the realization that the counterion effect is a complex function of the nature, strength, and extent of the interactions within the blend matrix. The very large elongation at break in the 5B-Ni blend might also be indicative of a morphology in which the rubbery phase is continuous or nearly so. This might arise as a consequence of the blend preparation processing. This remains speculative in the absence of definitive morphological information for the blends.

Fracture Surface Morphologies. Figure 8 shows the SEM micrographs of the freeze fractured surfaces of the blends. The 5B-Li and 5B-Na blends clearly exhibit a macrophase-separated morphology. The transition metal containing blends, on the other hand, exhibit relatively smooth surfaces which provides further evidence that compatibility is achieved. However, the roughened surface features observed for the 5B-Ca blend, which clearly differ from the macrophase-separated morphologies in the 5B-Li and 5B-Na blends, offer evidence for a degree of interfacial adhesion in this blend and perhaps a morphological difference between it and the group I metal containing blends.

Crystallization and Melting Behavior. The crystallization and melting behavior of the semicrystalline ionomers are compared and contrasted before and after blending. Consecutive heating and cooling cycles were performed on both the quenched ionomers and the blends. The transition temperatures and the corre-

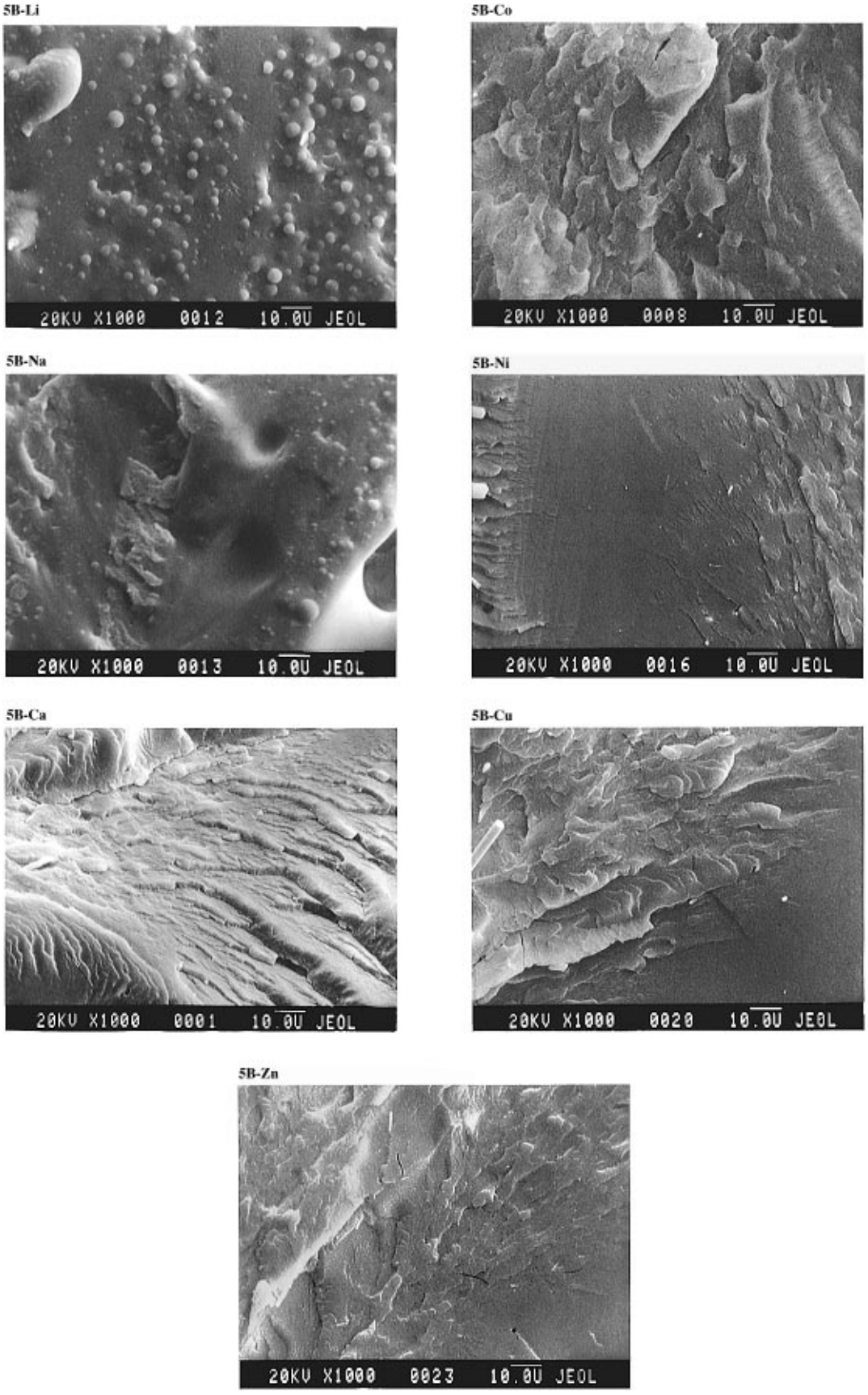

Figure 8. SEM micrographs for freeze fracture surfaces of solution-cast blends of 5B-M.

sponding enthalpy changes are recorded in Table 6. During the heating cycle, only the Li, Na, and Zn ionomers undergo cold crystallization followed by melting at higher temperatures. The 5B-Li, 5B-Ca, 5B-Co, and 5B-Cu blends behave similarly during heating. During the cooling cycle, crystallization is observed only for the zinc ionomer. It is apparent that the crystallization behavior of the ionomers is influenced to various extents by the different counterions present and the mixing between the ionomers and the 5EAVP polymer.

Table 6. DSC Results: Thermal Behavior during Heating/Cooling Scans

	heating				cooling	
polymer	T_c (°C)	ΔH_c (J/g)	T_m (°C)	ΔH_m (J/g)	T_c (°C)	ΔH_c (J/g)
5EAVP/4PET-SO_3Li-45/55	174	−2	206	2		
5EAVP/4PET-SO_3Na-45/55						
5EAVP/4PET-SO_3Ca-45/55	169	−4	207	2		
5EAVP/4PET-SO_3Co-45/55	151	−11	201	11		
5EAVP/4PET-SO_3Ni-45/55						
5EAVP/4PET-SO_3Cu-45/55	156	−4	201	2		
5EAVP/4PET-SO_3Zn-45/55						
4PET-SO_3Li	149	−23	205	21		
4PET-SO_3Na	139	−25	206	27		
4PET-SO_3Ca						
4PET-SO_3Co						
4PET-SO_3Ni						
4PET-SO_3Cu						
4PET-SO_3Zn	136	-24	212	26	154	−22

Table 7. DSC Results: Crystallization Kinetics and Melting Behavior Studies

		melting transitions (°C)			degree of crystallinity	
polymer	$t_{1/2}$ (min)	T_1	T_2	T_3	ΔH_m (J/g)	%
5B-Li	8.0	162	194	206	26	23
5B-Na	21.5	162	195	205	24	21
5B-Ca	14.2	164	195	206	25	22
5B-Co	14.3	161	195	204	23	21
5B-Ni	15.5	161	194	203	23	21
5B-Cu	17.8	161	194	205	25	22
5B-Zn	16.0	161	195	204	24	21
4PET-SO_3Li	7.5	163	195	205	28	25
4PET-SO_3Na	20.8	161	192	206	29	26
4PET-SO_3Ca	*a*		196		3	3
4PET-SO_3Co	*a*		197		8	7
4PET-SO_3Ni	*a*		197		2	2
4PET-SO_3Cu	*a*	170	196		14	12
4PET-SO_3Zn	21.1	171	198	209	25	22

[a] The crystallization time is beyond the experimental time frame.

However, due to the widely different crystallization rates of the individual blends and ionomers, their crystallization behavior could not be fully characterized under the current experimental conditions.

Isothermal crystallization was carried out on the amorphous blends and ionomers. The crystallization temperature T_c was chosen as 150 °C, a temperature at which the crystallization process can be fully characterized. At the end of the process, the isothermally crystallized samples were heated to their molten state to determine the melting behavior. Table 7 summarizes the results of the crystallization kinetics and melting behavior studies. The crystallization half-time $t_{1/2}$, defined as the time required to attain half of the total crystallinity, is used as a measure of the rate of crystallization at a particular T_c.

Results show that the crystallization rate of the ionomers is highly dependent upon the counterions in that the Li, Na, and Zn ionomers crystallize fairly rapidly while the rest of them do not complete the process within the experimental time frame. Studies have shown that ionic groups located at polymer chain ends accelerate the overall crystallization rate of the polymer by providing specific sites for nucleation.[18−20] Based on such findings, the different crystallization rates observed in the PET ionomers are ascribed to the difference in the nucleation efficiency of the metal-

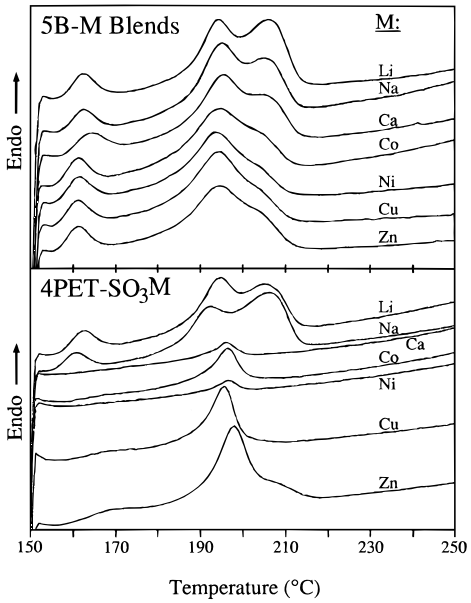

Figure 9. DSC thermograms showing the melting behavior of the isothermally crystallized samples of 5B-M blends and 4PET-SO_3M homopolymers.

neutralized ionic groups that are incorporated along the chain backbone. Comparing the $t_{1/2}$ values of the ionomers with their corresponding blends, it is noted that the crystallization rate of the Li and Na ionomers remains virtually the same after blending, while in the case of Zn, the rate is slightly enhanced in the blend. The invariant crystallization rate of the Li and Na ionomers provides additional evidence that both blends are strongly phase separated. Unlike the Zn ionomer, the crystallization rates of the Ca, Co, Ni, and Cu ionomers are significantly enhanced upon blending with the 5EAVP homopolymer to the extent that their $t_{1/2}$ values can be successfully determined within the experimental time frame. Our previous findings have shown that transition metal complexation between functionalized polymer chains is more effective in accelerating the crystallization process by offering more stable and efficient nucleating sites.[2] Hence, the dramatic rate enhancement in the transition metal containing blends as compared to their corresponding ionomers is attributed to the presence of strong complexation between the two polymer phases. However, in the case of the Ca ionomer, a similar rate enhancement is observed in the blend despite the absence of strong ionic complexation as demonstrated by the transition metal containing blends. A possible explanation could be due to the presence of ion−dipole interactions between the highly charged Ca^{2+} ion of the ionomer phase and the polar moieties of the 5EAVP phase, which results in an increase in nucleation efficiency. Moreover, such a finding helps to confirm that, unlike the Li and Na ionomers, there is indeed some interfacial interaction between the Ca ionomer and the 5EAVP, which leads to the enhancement of its modulus and the modification of the crystallization behavior of the ionomer in the blend.

Figure 9 shows the melting behavior of the isothermally crystallized ionomers and the blends. The melting transitions and the degree of crystallinity attained are recorded in Table 7. It should be noted that the observed multiple melting endotherms of the ionomers are typical of that for semicrystalline PET.[21] The thermal scans have shown that the population of

crystals formed can be divided into three main groups according to their melting transition temperatures: 160, 195, and 205 °C; the relative proportion of which varies with the counterion of the ionomer and also its interactions with the 5EAVP polymer. In the case of the Li and Na ionomers, the melting behavior remains almost unchanged after blending as is typical of macrophase-separated blends. For ionomers containing the divalent metal ions, the majority of the crystals melts at around 195 °C. However, the degree of crystallinity attained is strongly dependent on the nature of the counterion. As mentioned before, the crystallization of some of the ionomers is so slow that the whole process cannot be fully observed within the experimental time frame. Therefore, the observed degree of crystallinity is partially determined by the kinetics of the process, and the value should not be treated as an equilibrium quantity. Upon blending, the crystal population becomes as diverse as that of the 5B-Li and 5B-Na blends except that the crystals are less perfect as shown by a relatively lower contribution to the endothermic transition at around 205 °C. In addition, the degree of crystallinity attained is significantly enhanced as a result of the ionic interactions in the blend matrix, which helps to increase the crystallization rate. Moreover, it is interesting to note that both the extent of crystallization and the melting behavior of the ionomers become less dependent on the counterions in the blends than in the PET-SO_3M polymers themselves.

Conclusions

The effects of counterions on the phase behavior and mechanical properties of an ionomeric blend of poly(ethyl acrylate-*co*-4-vinylpyridine) with metal-neutralized sulfonated poly(ethylene terephthalate) is investigated. The nature of the specific intermolecular interactions between the vinylpyridine groups and the metal-neutralized sulfonate groups is examined by FTIR spectroscopy. Results show that the vinylpyridine complexes strongly with the transition metal ions which include Co^{2+}, Ni^{2+}, Cu^{2+}, and Zn^{2+}, and no interactions are found with Li^+ or Na^+. In the case of Ca^{2+}, some evidence exists for enhanced interfacial adhesion, probably due to ion−dipole interactions. Compatibility is observed for the transition metal containing blends as evidenced by their glass transition behavior probed by DSC and DMTA. The relative extent of compatibility is assessed by the amount of interfacial material present. The ultimate tensile properties of the transition metal containing blends exhibit significant improvement relative to the non-transition metal containing blends due to the lack of favorable interfacial adhesion via specific intermolecular interactions in the latter. However, the relative extent of property enhancement among the compatiblized blends is found to be a complex function of the nature, strength, and extent of transition metal complexation within the blend matrix. There is some indication that the Ca^{2+} and the transition metal containing blends exhibit a cocontinuous morphology while the Li^+- and Na^+-containing blends have a dispersed glassy phase in a rubbery matrix. On the other hand, the crystalline behavior of the PET ionomers exhibits a strong dependence on both the counterions and their interactions with the 5EAVP polymer. The crystallization rate of the ionomers is significantly increased upon blending due to the enhanced nucleation efficiency derived from the ionic clusters of specific interacting sites. The crystalline morphology as indicated by the multiple melting transitions is also modified as a result of the interactions of the ionomers with the 5EAVP polymer.

Acknowledgment. The authors gratefully acknowledge the financial supports received from the Materials Research Laboratory at the University of Massachusetts, supported by the National Science Foundation and the Center for University of Massachusetts Industry Research on Polymers (CUMIRP).

References and Notes

(1) Ng, C.-W. A.; Lindway, M. J.; MacKnight, W. J. *Macromolecules* **1994**, *27*, 3027.
(2) Ng, C.-W. A.; MacKnight, W. J. *Macromolecules* **1994**, *27*, 3033.
(3) Ng, C.-W. A.; MacKnight, W. J. *Macromolecules* **1996**, *29*, 2412.
(4) Peiffer, D. G.; Duvdevani, I.; Agarwal, P. K.; Lundberg, R. D. *J. Polym. Sci., Polym. Lett. Ed.* **1986**, *24*, 581.
(5) Agarwal, P. K.; Duvdevani, I.; Peiffer, D. G.; Lundberg, R. D. *J. Polym. Sci., Polym. Phys. Ed.* **1987**, *25*, 839.
(6) Lu, X.; Weiss, R. A. *Macromolecules* **1991**, *24*, 5763.
(7) Belfiore, L. A.; Pires, A. T. N.; Wang, Y.; Graham, H.; Ueda, E. *Macromolecules* **1992**, *25*, 1411.
(8) Belfiore, L. A.; Graham, H.; Ueda, E. *Macromolecules* **1992**, *25*, 2935.
(9) Belfiore, L. A. *Polym. Mater. Sci. Eng.* **1993**, *68*, 310.
(10) Douglas, E.; Sakurai, K.; MacKnight, W. J. *Macromolecules* **1991**, *24*, 6776.
(11) The elemental analysis was performed at the Microanalysis Laboratory at the University of Massachusetts, Amherst.
(12) Brandrup, J.; Immergut, E. H. *Polymer Handbook*, 3rd ed.; Wiley: New York, 1989; p v73.
(13) Ostrowska-Czubenko, J.; Ostrowska-Gumkowska, B. *Eur. Polym. J.* **1988**, *24* (1), 65.
(14) Beckman, E. J.; Karasz, F. E.; Porter, R. S.; Hunsel, J. Van; Koningsveld, R.; MacKnight, W. J. *Macromolecules* **1988**, *21* (4), 1193.
(15) McCrum, N. G. *J. Polym. Sci.* **1958**, *27*, 555.
(16) McCrum, N. G. *J. Polym. Sci.* **1959**, *34*, 355.
(17) McCrum, N. G. *Makromol. Chem.* **1959**, *34*, 50.
(18) Legras, R.; Bailly, C.; Daumerie, M.; Dekoninck, J. M.; Mercier, J. P.; Zichy, V.; Nield, E. *Polymer* **1984**, *25*, 835.
(19) Legras, R.; Dekoninck, J. M.; Vanzieleghem, A.; Mercier, J. P.; Nield, E. *Polymer* **1986**, *27*, 109.
(20) Dekoninck, J. M.; Legras, R.; Mercier, J. P. *Polymer* **1989**, *30*, 910.
(21) Roberts, R. C. *Polymer* **1969**, *10*, 113.

MA950974P